Optimisation of Magnetic Circuit for Brushless Doubly Fed Machines

Abdi Jalebi, S., Abdi, E., Oraee, A. & McMahon, R.

Original citation & hyperlink:
Abdi Jalebi, S, Abdi, E, Oraee, A & McMahon, R 2015, 'Optimisation of Magnetic Circuit for Brushless Doubly Fed Machines' *IEEE Transactions on Energy Conversion*, vol. 30, no. 4, pp. 1611-1620.
https://dx.doi.org/10.1109/TEC.2015.2468063

DOI 10.1109/TEC.2015.2468063
ISSN 0885-8969

Publisher: Institute of Electrical and Electronics Engineers (IEEE)

Optimisation of Magnetic Circuit for Brushless Doubly Fed Machines

Salman Abdi, Ehsan Abdi, *Senior Member, IEEE,* Ashknaz Oraee, and Richard McMahon

***Abstract*— This paper presents an optimised design method for the magnetic circuit of Brushless Doubly Fed Machines (BDFMs). The BDFM is an attractive electrical machine particularly for wind power applications as a replacement for doubly fed slip-ring generators. This study shows that the conventional design methods for the BDFM stator and rotor back iron can be modified, leading to a lighter and smaller machine. The proposed design concepts are supported by analytical methods and their practicality is verified using 2-D Finite Element (FE) modelling and analysis. Two BDFMs with frame sizes D180 and D400 are considered in this study.**

***Index Terms*— Brushless doubly fed machine (BDFM), finite element analysis (FEA), magnetic circuit, magneto motive force (MMF), total harmonic distortion (THD)**

I. Introduction

The Brushless Doubly Fed Machine (BDFM) shows commercial promise as both a variable speed drive and generator. As a generator, it is particularly attractive for wind power generation as a replacement for doubly-fed slip-ring generators which was first proposed by [1] and subsequent interest has been mainly focused on this application [2], [3]. A wind turbine incorporating a BDFM will have higher reliability and lower maintenance costs by virtue of the absence of brush-gear [4]. Studies have shown that problems with brush-gear are a significant issue in wind turbine operation and reliability, and that the problem will be more severe in machines deployed offshore where there are stronger winds and accessibility is impaired. In addition, the BDFM offers a key advantage as a variable speed drive in that it requires only a fractionally rated converter.

The BDFM has its origins in the self-cascaded machine [5] and comprises two electrically separate stator windings of different pole numbers, one connected directly to the grid, called the power winding (PW), and the other supplied from a variable voltage and frequency converter, called the control winding (CW). A schematic of the BDFM and the way it is connected to the grid is shown in Fig. 1. The pole numbers are selected in a way to avoid direct transformer coupling between the stator windings. The rotor winding is then specially designed to couple both stator windings. The machine is normally run in a synchronous mode, with an appropriate controller, in which the shaft speed is set by the frequencies supplied to the stator windings [6]. In this mode, the BDFM operates in a similar way to the doubly-fed induction generator with the torque related to the load angle and a grid side power factor which can be varied by adjusting the control winding voltage [7].

S. Abdi, A. Oraee and R. McMahon are with the Electrical Engineering Division, Cambridge University, Cambridge, CB3 0FA, UK (e-mail: s.abdi.jalebi@gmail.com; ram1@eng.cam.ac.uk)

E. Abdi is with Wind Technologies Limited, St Johns Innovation Park, Cambridge CB4 0WS, UK. (e-mail: ehsan.abdi@windtechnologies.com)

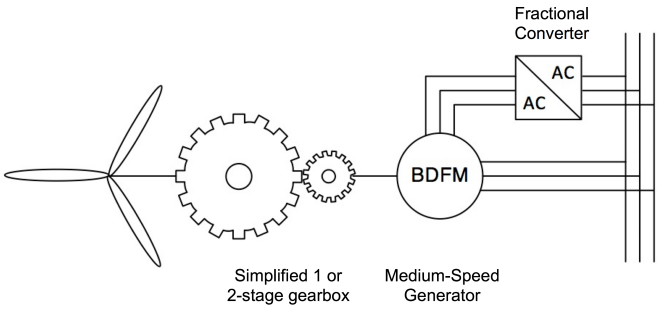

Fig. 1: Schematic of BDFM grid connection.

Fig. 2: 250 kW D400 BDFM (right front) on test bed.

To date, there have been several attempts to manufacture large BDFMs, for example in Brazil with a 75 kW machine [8], China with the design of a 200 kW machine [9] and the 250 kW BDFM reported by the authors in [10] and [11], shown in Fig. 2 on test bed. The latter was built in a frame size D400, as a stepping-stone towards a megawatt scale BDFM wind turbine. It is therefore desirable to optimise the weight and size of the machine before a large-scale BDFM is constructed, making it possible to retrofit the BDFM in existing wind turbines.

It was shown in [12] that the rotor flux density peak values in different teeth are not equal and vary according to a sinusoidal function. A similar pattern exists for the rotor core back sections. In this study, it is shown analytically that

the rotor field distribution does not depend on the operating speed and that the peak flux density in different sections of the rotor including teeth and back iron sections varies with angular position. Therefore, some parts of the rotor back iron which do not effectively contribute in the machine magnetic circuit can be removed to reduce its weight. Performance results from the new rotor are obtained in simulation and compared to the original design.

It is also shown in this paper that the proposed analytical calculation of the BDFM stator back iron by [13] leads to overestimation of the back iron depth. This is because it is considered that the BDFM stator back iron needs to be deep enough to carry two separate $2p_1$ and $2p_2$ pole magnetic fluxes. however, the BDFM magnetic field pattern has no obvious polar symmetry and the motion of the field is not a simple rotation. An alternative analytical method is proposed for the stator back iron calculation and is validated by FE analysis, leading to an optimised value for the stator back iron depth.

II. Prototype Machines Considered in This Study

The specifications of the prototype BDFMs used in this study are shown in Table I. These BDFMs have 4 and 8 pole stator windings and were constructed in frame sizes 400 and 180 with the stack length of 820 mm and 190 mm, respectively. The stator windings in both machines were connected in delta. The rotors comprise six sets of nests each consisting concentric loops [14], the conductors being solid bars with one common end ring [15]. The magnetic properties for the iron were provided by the machine manufacturer.

TABLE I: Specifications of the prototype BDFMs

Frame size	400	180
PW pole number	4	4
PW rated voltage	690V at 50 Hz (delta)	240V at 50 Hz (delta)
PW rated current	178 A (line)	9.5 A (line)
CW pole number	8	8
CW rated voltage	620 V at 18 Hz (delta)	172 V at 25 Hz (delta)
CW rated current	73 A (line)	6.8 A (line)
Speed range	500 rpm ±36%	750 rpm ±33%
Rated torque	3670 Nm	100 Nm
Rated power	250 kW at 680 rpm	7.8 kW at 750 rpm
Efficiency (at full load)	> 95%	> 92%
Stack length	0.82 m	0.19 m

III. Rotor Magnetic Circuit Optimization

A. Variation of Peak Flux Density with Angular Position

A study was performed by Creedy et. al. [16] on the BDFM magnetic field characteristics, which found that the peak values of the rotor MMF are not equal in all parts of the rotor and vary sinusoidally with angular positions. This observation was used later by Liao et. al. [17] to design a BDFM with reluctance rotor. Williamson et. al. in [18] found by performing FE analysis that the movement of the field is not a matter of simple rotation and does not have a distinguishing N-S pattern.

The characteristic of the BDFM field distribution, generated by its stator and rotor windings, is represented by equation (1) using the flux density distribution for different combinations of f_1 and f_2 [19]. In this equation the effects of iron saturation, slotting effects, and finite distributions of windings conductors are ignored:

$$B(\theta,t) = \hat{B}_1 \cos(2\pi f_1 t - p_1\theta) + \hat{B}_2 \cos(2\pi f_2 t - p_2\theta + \alpha) \quad (1)$$

where:

- $\hat{B}_1$ and $\hat{B}_2$ are the peak flux density values, in T, of the $2p_1$-pole and $2p_2$-pole flux density waveforms, respectively.
- f_1 and f_2 are the excitation frequencies, in Hz, of the $2p_1$-pole and $2p_2$-pole flux density waveforms, respectively.
- t is time in seconds (s).
- θ is the angular position with a range of $[0^o : 360^o)$
- α is the phase angle offset and its value sets the relative alignment of the $2p_1$ and $2p_2$ pole flux density distributions and it can only be modified by changing the stator windings excitation phase angles because the relative positions of the windings are fixed.

The field distribution components in the rotor frame can be obtained from (1) when

$$f_1 = f_2 \quad (2)$$

This is true when the $2p_1$-pole and $2p_2$-pole fields distribution components rotate in the same direction relative to the rotor, known as 'Cumulative BDFM', which is the preferred BDFM type [5]. However, the values of f_1 and f_2 for the stator field distribution components are related to the BDFM speed given by:

$$N = 60\frac{f_1 \pm f_2}{p} \quad (3)$$

where N is the shaft speed in rev./min. and p is either equal to $p_1 + p_2$ or $p_1 - p_2$ for the cumulative and differential BDFM, respectively. Therefore, the stator field distribution depends on the operating speed and that of the rotor does not. Equation (1) can be reduced to the sum of traveling and standing waves when $f_1 = f_2$.

$$\begin{aligned} B(\theta,t) = \; & 2B_1 \cos(2\pi f_1 t - \frac{p_1+p_2}{2}\theta) \times \cos(\frac{p_2-p_1}{2}\theta) \\ & + (B_2 - B_1)\cos(2\pi f_1 t - p_2\theta) \end{aligned} \quad (4)$$

The peak value of (4) is not equal for different angular positions because of the standing wave term, i.e.:

$$2B_1 \cos(\frac{p_2-p_1}{2}\theta) \times \cos(2\pi f_1 t - \frac{p_1+p_2}{2}\theta) \quad (5)$$

whose amplitude at different θ is not equal and varies sinusoidally. It can be therefore concluded that the rotor field distribution does not depend on the operating speed and, in addition, the peak flux density in different sections of the rotor including different rotor teeth and back iron sections varies with angular position as the absolute value of a sinusoidal function. This fact is further investigated by performing time-stepping finite element simulation in the next section.

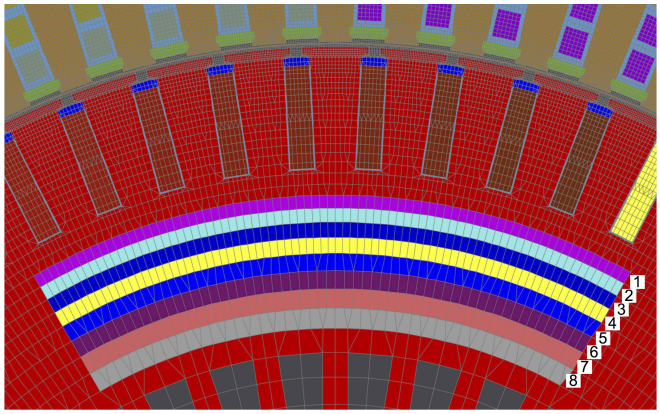

Fig. 3: Meshing of the rotor back iron; Different colours show different distance from the centre.

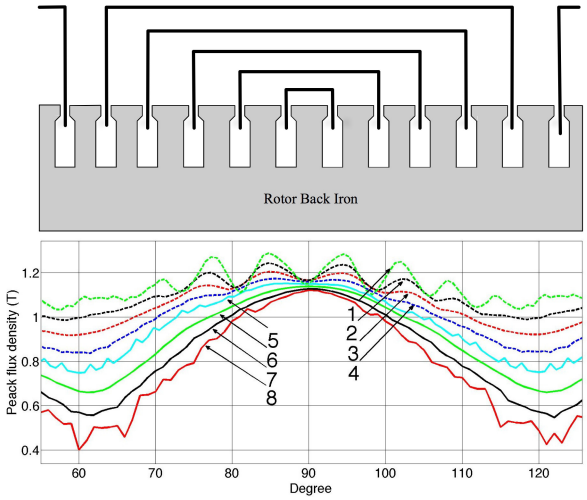

Fig. 4: The peak flux densities in the rotor back iron elements specified with different numbers in Fig. 3

B. Finite Element Analysis of Rotor Field Distribution

The D400 BDFM is modelled in its synchronous operating mode, using time-stepping finite element (FE) simulation taking the material nonlinear characteristics into account. The operating conditions are as described in Table II. The rotor is a nested loop design with six nests, each comprising five loops. Because the flux pattern in a BDFM has 180^o symmetry, only half of the machine cross section is analysed [20].

The rotor back iron meshing for a single nest span i.e. 60^o is shown in Fig. 3. The elements with the same colour have the same distance from the rotor centre. The peak flux density for each colour group is calculated and shown in Fig. 4. As can be seen, the peak flux density in rotor back iron is highest and lowest in the centre of each nest and between two adjacent nests, respectively. In addition, the regions closer to the rotor shaft have much higher variation in the peak flux density. Thus, larger weight reduction can be achieved closer to the shaft.

C. A New Rotor Back Iron Design For the BDFM

A new back iron design has been proposed for the rotor based on the flux distribution discussed above. The cross

TABLE II: The prototype BDFMs operating conditions considered in this study

BDFM Frame Size	*D*400	*D*180
Torque(Nm)	3600	103
Speed (rev/min)	650	750
$\lvert V_{4-pole}\rvert$ (V)	690	240
f_{4-pole} (Hz)	50	50
$\lvert V_{8-pole}\rvert$ (V)	606	175
f_{8-pole} (Hz)	15	25

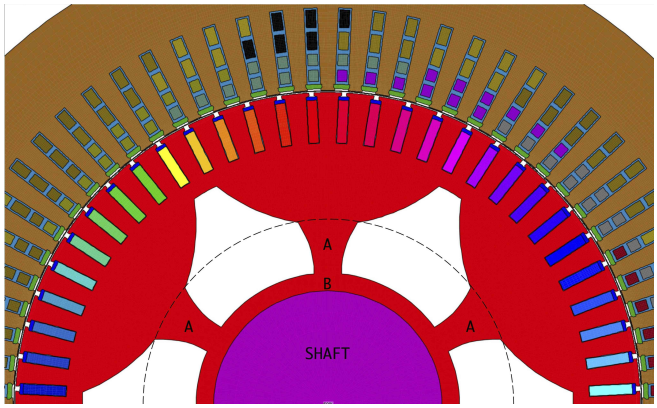

Fig. 5: The cross section of the new designed rotor for D400 BDFM.

section of the new design for the D400 BDFM rotor is shown in Fig. 5. There are two region inside the dashed circle, *A* and *B*, which do not take part in the magnetic circuit, and therefore their design is mainly driven by mechanical restrictions and cooling requirements, which is outside the scope of this paper.

The back iron region outside the dashed circle forms part of the rotor magnetic circuit and therefore its design affects the machine performance. As can be seen in Fig. 5, the regions further from nest centre have thiner back iron depth since they carry less magnetic flux. In the following sections, the magnetic characteristics and performance of the machine will be assessed for synchronous and induction modes of operations.

1) Synchronous mode of operation: The D400 BDFM is operating in its synchronous mode of operation and at the same operating conditions given in Table II. No noticeable change was found in the values of stator currents and machine torque when the new back iron design is used. In order to assess the flux density in the new back iron design, the peak flux density in the elements shown in green in Fig. 6 are plotted in Fig. 7. As can be seen, the peak flux densities are below 1.8 *T* which is the design limit.

Fig. 8 shows the modulus of flux density and magnetic flux lines when the BDFM is run in synchronous mode of operation with its rated supplied voltages and rated frequencies as given in Table II. As it can be observed, in the normal operating mode and under rated conditions, no excessive saturation can

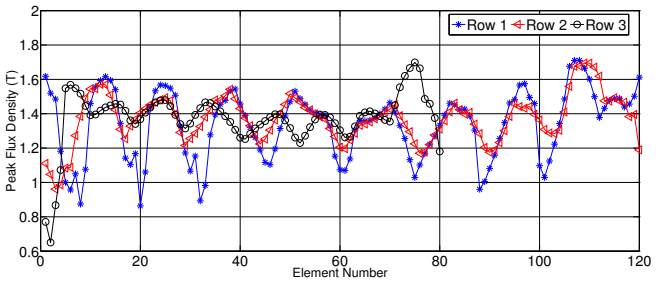

(a) Peak flux density values in rows 1, 2, and 3

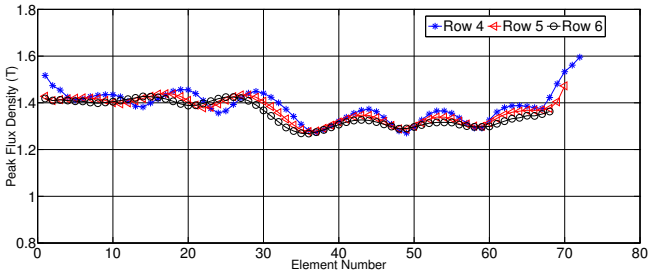

(b) Peak flux density values in rows 4, 5, and 6

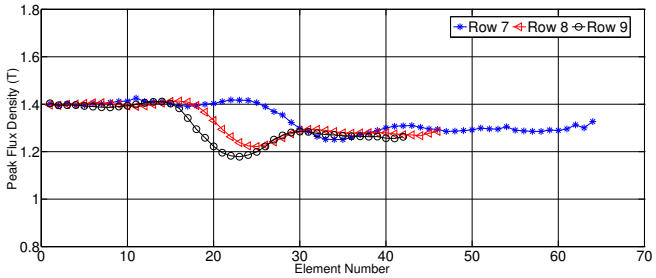

(c) Peak flux density values in rows 7, 8, and 9

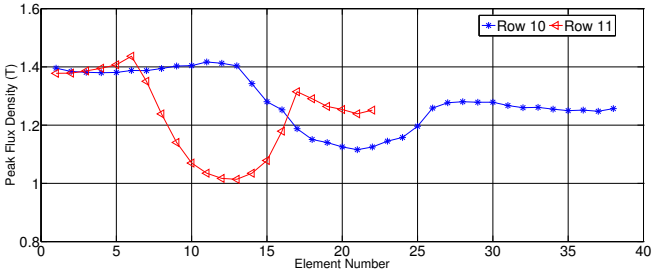

(d) Peak flux density values in rows 10 and 11

Fig. 7: The peak flux density values in new designed rotor back iron elements. The row numbers are corresponding to the numbers specified in Fig. 6

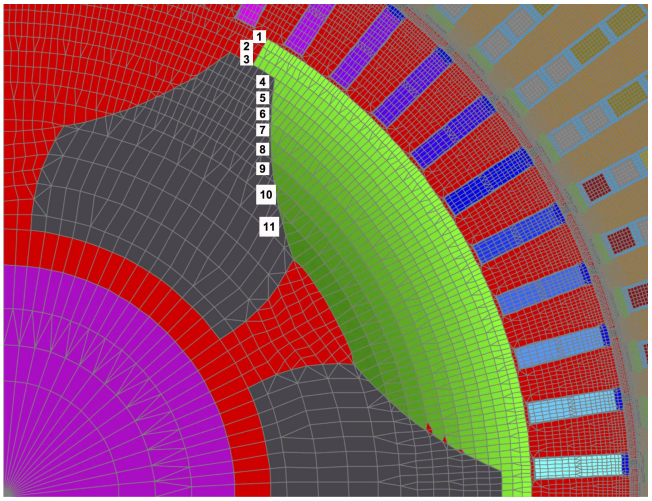

Fig. 6: Rows of elements between two chunks of the new designed rotor back iron specified with different green colours.

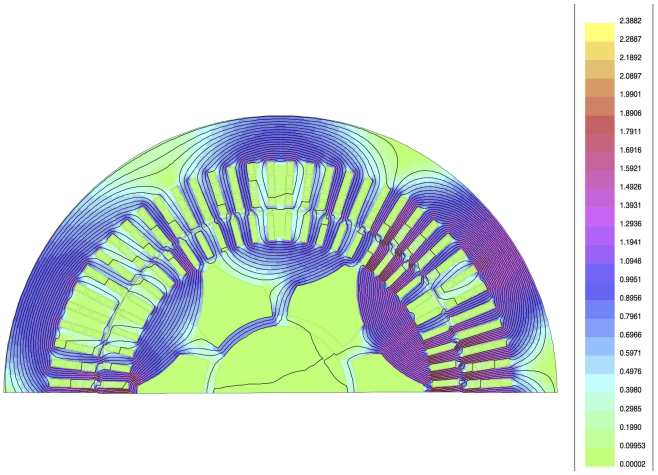

Fig. 8: Numerical computation of flux density magnitude colour map with flux line overlaid; for the D400 BDFM in synchronous mode of operation, obtained from FE non-linear analysis

be found in machine iron regions confirming the practicality of the new design method for rotor back iron.

2) Induction mode of operation: The D400 BDFM with the new rotor design has been modelled in induction mode of operation using FE analysis in order to assess its magnetising characteristics. When only one stator winding is supplied and the unsupplied winding is left open, the BDFM operates as an induction machine and if the rotor speed is set to the synchronous speed, only the field due to the excited winding will exist and hence, the BDFM magnetising characteristics can be assessed.

Figs. 9 (a) and (b) show the stator CW and PW magnetising characteristics obtained from the FE model. The rated PW and CW voltages at which PW and CW rated magnetic fields are achieved at the excited frequencies, can be calculated from the following equations [21]:

$$\left|V_{rms}^{CW}\right| \simeq ld\omega_{CW}N_{ph}^{CW}k_w^{CW}B_{rms}^{CW} \tag{6}$$

$$\left|V_{rms}^{PW}\right| \simeq ld\omega_{PW}N_{ph}^{PW}k_w^{PW}B_{rms}^{PW} \tag{7}$$

where l is the machine stack length, d is the mean air gap diameter, ω is the supply angular frequency, N_{ph} is the number of turns per phase per pole pair, K_w is the winding factor, and B_{rms} is the rms value of a stator winding rated magnetic flux. The V_{rms}^{CW} and V_{rms}^{PW} are calculated for D400 BDFM as 356 V

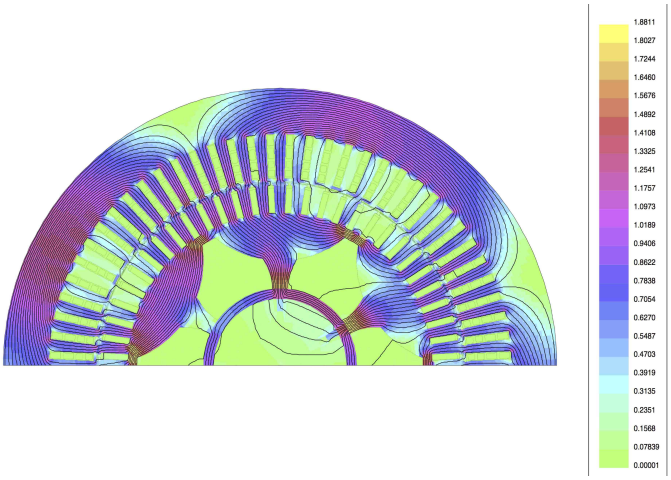

Fig. 10: Numerical computation of flux density magnitude colour map with flux line overlaid; for the D400 BDFM in PW induction mode of operation, obtained from FE non-linear analysis. The PW voltage and frequency are set to 400V and 20Hz, respectively.

and 284 V and shown in Fig. 9 (a) and (b) by solid horizontal lines, respectively.

As can be seen from Fig. 9a, the CW magnetising characteristic is similar for the original and the new back iron designs. From Fig. 9b, the PW shows similar agreement below its rated voltage (solid line), but when the voltage is set to a greater value, heavy saturation occurs. As can be seen from Fig. 10 which shows the modulus of flux density and magnetic flux lines at 400 V, 20 Hz, since the 4-pole span is wider than the nest span, the flux lines force their way through the narrow parts of the new back iron which causes heavy saturation. However, in real operating conditions, in the synchronous mode, none of the stator PW and CW is required to provide substantially higher flux density than its rated design value, hence, the saturation condition mentioned above is not occurred.

IV. Stator Magnetic Circuit Optimization

A. BDFM Specific Magnetic Loading

For a typical induction machines, designers use the specific magnetic loading, based on the electrical steel chosen, to achieve a balance between the effective use of the iron and undue saturation [22]. However, evaluating the overall effect of the BDFM's two stator fields, with rms flux densities of B_1 and B_2 on its iron circuit, is not straightforward as the magnetic flux circulating in the BDFM is complex [7].

The conventional explanation for the operation of the BDFM considers two independent flux systems related to the power and control windings. However, in a BDFM the fluxes are coupled via the rotor and the flux circulating in the machine is the resultant of MMFs from the three windings acting on their side of the air gap: The explicit MMF waves of p_1 and p_2 pole pairs of the stator power and control windings, and the implicit MMF wave from the rotor winding with components of p_1 and p_2 pole pairs plus space harmonic content depending on the degree of distribution of the rotor winding. The resulting air gap flux then comprises components of p_1 and p_2 pole pairs, plus space harmonics.

The specific magnetic loading is traditionally defined as the mean absolute flux per pole in the air gap of a machine [23]:

$$\bar{B} = \lim_{T\to\infty} \frac{1}{T}\int_0^T \frac{1}{2\pi}\int_0^{2\pi} \left|B(\theta)\right| \, d\theta \, dt \tag{8}$$

where $B(\theta)$ is the flux density in the air gap, assumed uniform along the axis of the machine. Ignoring the harmonic fields, the magnetic field in the air gap of the BDFM may be written using (1) as:

$$B(\theta) = \sqrt{2}B_1 \cos(\omega_1 t - p_1\theta) + \sqrt{2}B_2 \cos(\omega_2 t - p_2\theta + \alpha) \tag{9}$$

where α is an arbitrary phase offset. It was shown in [7] that the magnetic loading of the BDFM regardless of the pole number combinations can be defined as:

$$\bar{B} = \frac{2\sqrt{2}}{\pi}\sqrt{B_1^2 + B_2^2} \tag{10}$$

B. Stator Back Iron Flux Densities

The maximum flux densities in the teeth and core back must be chosen according to design criterion e.g. to avoid saturation in the core, to minimise core losses, etc. The number of poles and magnetic loading determine the depth of the stator back iron in conventional single field electrical machines. For an induction machine, the back iron depth, y_c, is calculated as [23]:

$$y_c = \frac{\sqrt{2}Bd}{2p\bar{B}_c} = \frac{\bar{B}\pi d}{4p\bar{B}_c} \tag{11}$$

where p is the number of pole pair, $\bar{B}$ is the magnetic loading, $\hat{B}_c$ is the back iron maximum flux density, y_c is the core depth, and d is the air gap diameter. However, the BDFM has two stator windings with different pole numbers and hence the magnetic field pattern has no obvious polar symmetry and the motion of the field is not a simple rotation. As a result, the above equation can not be utilised for the BDFM. In [13] the back iron flux is modelled as the superposition of two fundamental back iron fluxes which are related to B_1 and B_2:

$$\begin{aligned} B_c(\theta,t) = \; & \frac{\sqrt{2}B_1 d}{2p_1 y_c}\cos(\omega_1 t + p_1\theta) \\ & + \frac{\sqrt{2}B_2 d}{2p_2 y_c}\cos(\omega_2 t + p_2\theta + \delta) \end{aligned} \tag{12}$$

where δ is the phase offset between the two back iron fluxes. As can be seen from (12), the back iron peak flux density at different angular locations is not the same because the progression of the 4 pole and 8 pole electrical angles is different. This brings difficulty in defining a single value as a measure of the back iron flux density. In [13] the back iron peak flux density is represented by the average value of maximum back iron flux densities found around the machine circumference over a period which is the smallest integer multiple of the period of the two supplies, given by:

$$\bar{B}_c = \frac{1}{T}\int_0^T max(B_c(\theta,t))\, dx \tag{13}$$

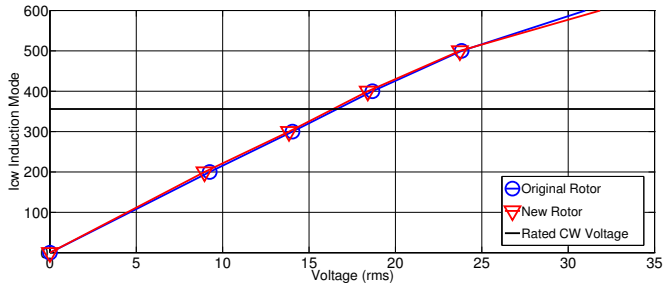

(a) CW magnetising characteristic at 10 Hz

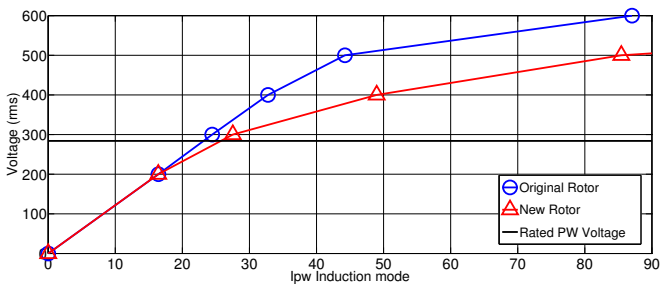

(b) PW magnetising characteristic at 20 Hz

Fig. 9: D400 BDFM magnetising characteristics with the new designed rotor. (a) the CW is supplied and PW is opened. (b) the PW is supplied and CW is opened.

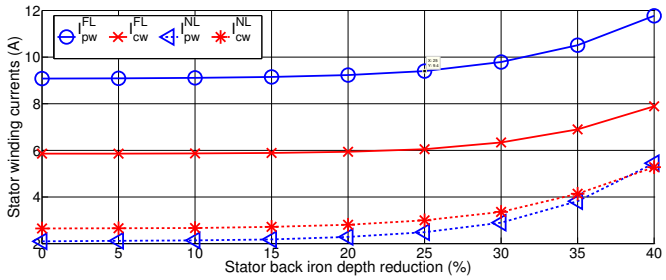

Fig. 11: PW and CW currents for D180 BDFM in synchronous mode of operation. The machine is run in Full-load ($T \simeq 100$ $N.m$) and No-load ($T \simeq 0$ $N.m$) conditions.

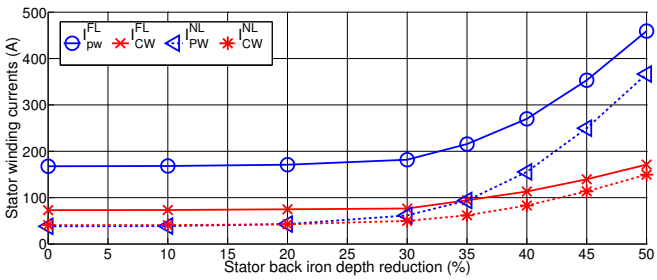

Fig. 12: PW and CW currents for D400 BDFM in synchronous mode of operation. The machine is run in Full-load ($T \simeq 3600$ $N.m$) and No-load ($T \simeq 0$ $N.m$) conditions.

The back iron depth of a BDFM is then considered as the sum of back iron depths needed to accommodate the two fundamental fluxes.

$$y_c = \frac{\sqrt{2}B_1 d}{2p_1\bar{B}_c} + \frac{\sqrt{2}B_2 d}{2p_2\bar{B}_c} = \frac{\sqrt{2}d}{2\bar{B}_c}\left(\frac{B_1}{p_1} + \frac{B_2}{p_2}\right) \qquad (14)$$

The FE analysis of D400 BDFM performed in synchronous mode of operation shows that the stator back iron depth obtained from (14) is considerably larger than the required depth to avoid saturation. In order to investigate potential weight reduction in the stator back iron, the performance of prototype BDFMs are analysed in their synchronous and induction modes of operation when their stator back iron depth is reduced. The stator PW and CW currents in synchronous operating mode and in full-load and no-load conditions are shown in Figs. 11 and 12 for D180 and D400 BDFMs, respectively. The PW and CW voltages and frequencies are as described in Table II.

As it is clear in Figs. 11 and 12, there are no significant increases in PW and CW currents in both full-load and no-load conditions when the core back length is reduced up to 30%. At this level of depth reduction, the maximum increase in a stator current from its rated value is below 5%. In order to see the effects of stator back iron depth reduction on machine magnetisation characteristics, D400 BDFM is modelled in the induction mode and results are shown in Fig. 13. The magnetising currents remain effectively unchanged in the range of interest, i.e. below rated voltage, when 30% reduction is applied to stator back iron depth. Therefore, from the above, 30% reduction in the stator back iron depth can be applied without affecting the performance of the prototype BDFMs, which were designed based on 14.

C. Stator Time Harmonics Consideration

Stator back iron depth reduction increases not only the stator current amplitudes, but also their harmonic contents. Total Harmonic Distortion (THD) is used to compare the level of harmonic content in the stator currents when different levels of back iron reduction is applied compared to the original design [24]. The THD for a stator current when j% reduction in stator back iron depth is applied can be defined as:

$$THD(I_j) = \frac{1}{I_{fund}}\sqrt{\sum_{i=1}^{n} I_j^2(f_i)} \qquad (15)$$

where f_i is the ith harmonic frequency, $I_j(f_i)$ is the current harmonic component at f_i, and I_{fund} is the fundamental component of the stator current. The PW and CW currents time harmonic components for D400 BDFM, in synchronous mode of operation and at full-load and no-load conditions, are shown in Figs. 14 and 15 respectively. The THD is also calculated for PW and CW currents for the above conditions, given in Table III. The harmonic levels are investigated when 0%, 30%, 40%, and 50% reduction in the back iron depth is applied. The levels of harmonic components for the cases of less than 30% depth reduction are very close to the original case and hence are removed from further consideration. In 30% reduction case, the THD is increased by up to 15% which

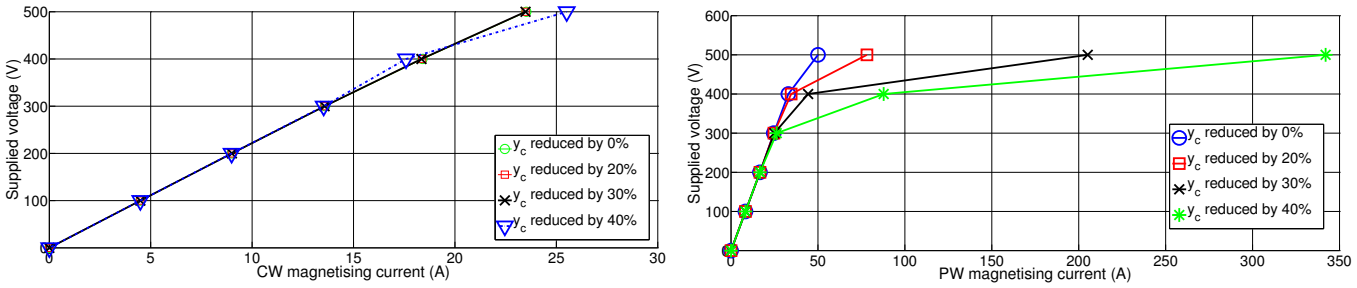

(a) CW magnetising current

(b) PW magnetising current

Fig. 13: D400 BDFM magnetising characteristics when different stator back iron reductions are applied. (a) the CW is supplied and PW is opened. (b) the PW is supplied and CW is opened.

is occurred in PW current at no-load condition, compare to 0% depth reduction case. The jump in THD levels for the cases of 40% and 50% depth reduction is high enough to make these cases thoroughly unacceptable.

TABLE III: THD calculated for PW and CW currents in full-load and no-load conditions when D400 BDFM operates in synchronous mode

Back Iron Depth Reduction	THD(%)			
	I_{PW}^{FL}	I_{CW}^{FL}	I_{PW}^{NL}	I_{CW}^{NL}
0%	10.6	8.6	18.9	17.2
30%	10.8	9.7	21.7	19.6
40%	11.8	15	33.1	36.5
50%	17.4	19.8	69.5	38.9

D. Stator Back Iron Depth Calculation

The core back depth required in an electrical machine is related to the number of poles and its magnetic loading. However, in a BDFM the magnetic field pattern has no clear polar symmetry i.e. it does not have a regular multi pole distribution. Furthermore, the motion of the field is not a matter of simple rotation. In this section the fundamental air gap MMF waves are employed to find the total MMF acting across the air gap. It will then be shown that the response of the BDFM rotor winding structure to that MMF determines the field pattern in the machine's iron region. Hence, the fundamental flux wave of the BDFM, can be defined by the (p_1+p_2)-pole rotor design, linking stator and rotor irons, rather than the $2p_1$ and $2p_2$ poles stator windings.

Assuming the MMF due to the stator windings PW and CW as MMF_{gs}, and the MMF due to the reaction of rotor winding as MMF_{gr}, the combined action of these MMFs sums to the total air gap MMF wave of MMF_g which develop the machine magnetic flux and therefore the rotor torque. The stator MMF acting on the air gap can be given as:

$$\begin{aligned} MMF_{gs} = \; & k_{w1}N_1I_1\cos(\omega_1 t - p_1\theta) + \\ & k_{w2}N_2I_2\cos(\omega_2 t - p_2\theta - \gamma) \end{aligned} \tag{16}$$

(16) can be resolved as:

$$\begin{aligned} MMF_{gs} = \; & 4k_{w1}N_1I_1\cos\gamma.\{\cos((\omega_1+\omega_2)t/2 + \\ & (p_1+p_2)\theta/2-\gamma)\}.\{\cos((\omega_1-\omega_2)t/2 + \\ & (p_1-p_2)\theta/2-\gamma)\} \end{aligned} \tag{17}$$

where:

$$\gamma = (\pi/2)(k_{w1}N_1I_1/k_{w2}N_2I_2) \tag{18}$$

The BDFM rotor winding must have $q = p_1 \pm p_2$ poles to meet the BDFM rules. Most prototype BDFMs have $q = p_1 + p_2$ poles on the rotor, because of difficulties in achieving acceptable performance with $q = p_1 - p_2$. MMF_{gr} in this case must take the form:

$$MMF_{gr} = k_{wr}N_rI_r\{\cos((\omega_1+\omega_2)t/2 + (p_1+p_2)\theta/2)\} \tag{19}$$

From (17) it can be seen that the MMF due to the stator consists of two waves, one with $p_1 + p_2$ pole pairs rotating at $(\omega_1 + \omega_2)/(p_1 + p_2)$ rad/sec and another of $p_1 - p_2$ pole pairs rotating at $(\omega_1 - \omega_2)/(p_1 - p_2)$ rad/sec. If a $q = p_1 + p_2$ pole rotor design is selected, the rotor reflects this action with an MMF given by (19). With this design therefore, the MMF acting across the air gap will be:

$$\begin{aligned} MMF_g = \; & MMF_{gs} - MMF_{gr} = \\ & 4k_{w1}N_1I_1\cos\gamma.\{\cos((\omega_1+\omega_2)t/2 + \\ & (p_1+p_2)\theta/2-\gamma)\}.\{\cos((\omega_1-\omega_2)t/2 + \\ & (p_1-p_2)\theta/2-\gamma)\} - k_{wr}N_rI_r\{\cos((\omega_1+\omega_2)t/2 + \\ & (p_1+p_2)\theta/2)\} \end{aligned} \tag{20}$$

The result is that the rotor structure can only respond to one of the two fundamental components of the stator MMF wave and the rotor suppresses the other stator MMF wave, with consequences to the PW and CW currents, resulting in end winding and air gap leakage effects. This ensures that the $(p_1 - p_2)/2$ wave effectively appears in the leakage path only. Therefore, the fundamental flux wave of the BDFM, can be defined by the q-pole rotor design, linking stator and rotor, and rotating at $(\omega_1 + \omega_2)/(p_1 + p_2)$.

Fig. 16 shows the magnetic flux in the iron circuit of D400 BDFM with 4/8-pole stator winding configuration. As can be seen in the figure, the magnetic field linking the stator and rotor iron has a 6-pole pattern as predicted above, although, all poles' flux strengths are not identical.

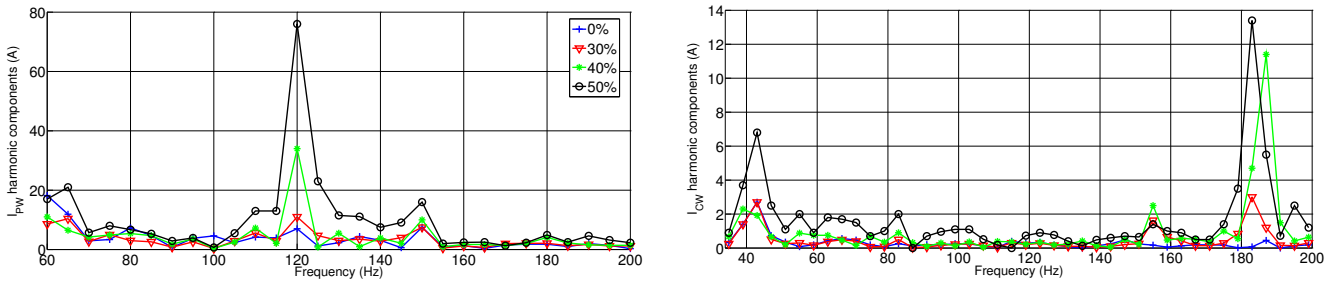

(a) PW current harmonic components

(b) CW currents harmonic components

Fig. 14: D400 BDFM stator (a) PW and (b) CW currents harmonic components when the machine operates at synchronous mode and full-load conditions.

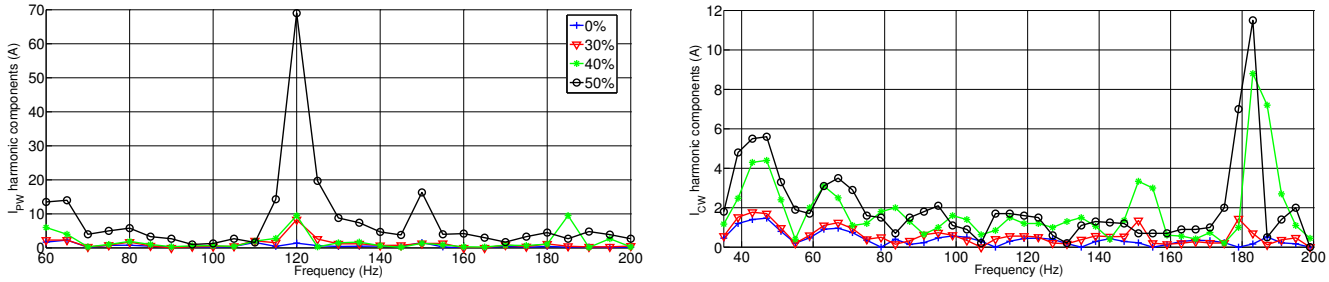

(a) PW current harmonic components

(b) CW currents harmonic components

Fig. 15: D400 BDFM stator (a) PW and (b) CW currents harmonic components when the machine operates at synchronous mode and no-load conditions.

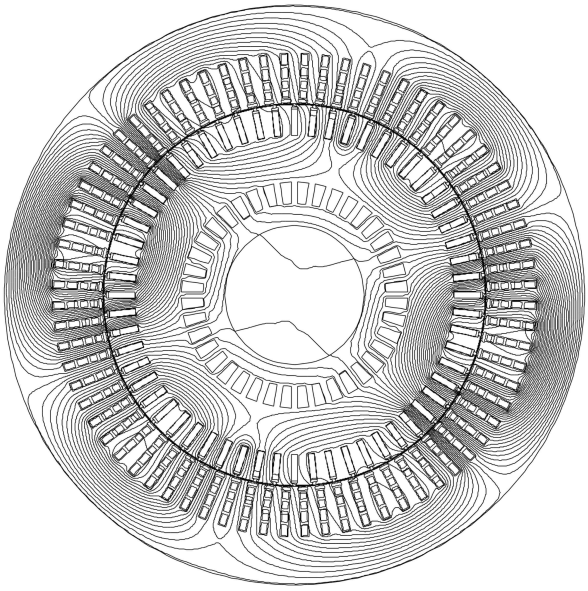

Fig. 16: Magnetic flux in the BDFM in synchronous mode of operation

This finding can be used to obtain an optimum design value for stator core back length if the BDFM is treated as an induction machine with p_1+p_2 poles and the magnetic loading of $\frac{2\sqrt{2}}{\pi}\sqrt{B_1^2+B_2^2}$. This is summarised in Table IV. The stator back iron depth in the new design method is about 32% and 31% smaller than in original design method in D180, and D400 BDFMs, respectively. This level of reduction has been shown in previous sections to be an acceptable limit before the machine is prone to saturation effects. The analytical method proposed in this section is based on the fundamental air gap MMF waves including the MMF due to the stator PW and CW, and the MMF due to the reaction of rotor winding, hence, it is generally valid for all BDFMs.

It should be noted that due to the excessive field harmonics existed in the machine main air gap field, mainly caused by slotting effects, stator winding configurations, and rotor nested loop structure; larger magnetic loading than the value obtained by (10) is expected for a BDFM. Consequently, in the machine design stage and when the back iron depth reduction is applied, non-linear FE analysis should be employed to assess the possibility of saturation in the machines magnetic circuit, specially in stator teeth and back iron.

TABLE IV: Comparison of two methods to calculate stator core depth, proposed by [13] and this paper

	y_c Term	y_c Value		Reduction in y_c	
		D180	D400	D180	D400
Old Design	$\frac{\sqrt{2}d}{2\hat{B}_c}\left(\frac{B_1}{p_1}+\frac{B_2}{p_2}\right)$	21.4(mm)	54.2(mm)	–	–
New Design	$\frac{\bar{B}\pi d}{4p\hat{B}_c}, p=p_1+p_2$,$\bar{B}=\frac{2\sqrt{2}}{\pi}\sqrt{B_1^2+B_2^2}$	14.5(mm)	37.4(mm)	32%	31%

V. Conclusions

In this study new design methods have been investigated for the BDFM in order to optimise its magnetic circuit, hence, reducing its size and weight. BDFMs are attractive machines for wind power generation as a replacement for doubly-fed slip-ring generators. It is therefore desirable to optimise the weight and size of the machine before a large-scale BDFM is constructed making it possible to retrofit the BDFM in existing wind turbines.

It has been shown that the peak flux density in the rotor magnetic circuit including rotor back iron varies with angular position, independent of the rotor speed. It has therefore been shown that some parts of the rotor back iron do not contribute in the machine magnetic circuit and hence can be removed to reduce its weight. This finding has been used to design a new rotor back iron in which $p_1 + p_2$ chunks were removed, reducing the rotor weight by about 20%.

This study also revealed that the conventional analytical methods for the BDFM stator back iron depth calculation lead to overestimations. It has been shown that the fundamental flux wave of the BDFM can be defined by the $(p_1 + p_2)$-pole rotor design, linking stator and rotor, and rotating at $(\omega_1 + \omega_2)/(p_1 + p_2)$. Therefore, an appropriate value for the back iron depth can be derived when a BDFM is considered as an induction machine with $(p_1 + p_2)$ pole pairs and the magnetic loading of $\frac{2\sqrt{2}}{\pi}\sqrt{B_1^2 + B_2^2}$. This value is 30% smaller than the proposed value by conventional methods, proved by FE analysis of two prototype BDFMs. The summary of results from the new design methods for both rotor and stator are shown in Table V, showing significant reduction in the total weight and size.

TABLE V: The reduction level in stator, rotor and total machine weights, and machine diameter in prototype BDFMs obtained by the new design methods

BDFM	Machine Diameter	Stator Weight	Rotor Weight	Total Weight
D180	4.7%	16.2%	20%	17.9%
D400	5%	17.5%	21%	18.8%

References

[1] A. Wallace, R. Spee, and G. Alexander, "Adjustable speed drive and variable speed generation systems with reduced power converter requirements." Budapest: ISIE IEEE international Symposium on Industrial Electronics, June 1993, pp. 503 – 508.

[2] C. S. Brune, R. Spee, and A. K. Wallace, "Experimental evaluation of a variable-speed, doubly-fed wind-power generation system," *IEEE Trans. Industry Applications*, vol. 30, no. 3, pp. 648 – 655, 1994.

[3] R. A. McMahon, X. Wang, E. Abdi-Jalebi, P. J. Tavner, P. C. Roberts, and M. Jagiela, "The bdfm as a generator in wind turbines." 12th International Power Electronics and Motion Control Conference, EPE-PEMC, September 2006.

[4] H. Arabian-Hoseynabadi, H. Oraee, and P. J. Tavner, "Wind turbine productivity considering electrical subassembly reliability," *Renewable Energy*, no. 35, pp. 190–197, 2010.

[5] A. R. W. Broadway and L. Burbridge, "Self-cascaded machine: A low-speed motor or high frequency brushless alternator," *IEE Proceedings*, vol. 117, pp. 1277–1290, 1970.

[6] S. Shao, E. Abdi, and R. McMahon, "Stable operation of the brushless doubly-fed machine (bdfm)." Bangkok, Thailand: Seventh International Conference on Power Electronics and Drive Systems, November 2007, pp. 897 – 902.

[7] R. A. McMahon, P. C. Roberts, X. Wang, and P. J. Tavner, "Performance of bdfm as generator and motor," *Electrical Power Applications, IEE Proceedings*, vol. 153, no. 2, pp. 289–299, March 2006.

[8] R. Carlson, H. Voltolini, F. Runcos, P. Kuo-Peng, and N. Baristela, "Performance analysis with power factor compensation of a 75 kw brushless doubly fed induction generator prototype." IEEE International Conference on Electric Machines and Drives, 2010.

[9] H. Liu and L. Xu, "Design and performance analysis of a doubly excited brushless machine for wind power generator application." IEEE International Sympousiom on Power Electronics for Distributed Generation Systems, 2010, pp. 597 – 601.

[10] E. Abdi, R. McMahon, P. Malliband, S. Shao, M. Mathekga, P. Tavner, S. Abdi, A. Oraee, T. Long, and M. Tatlow, "Performance analysis and testing of a 250 kw medium-speed brushless doubly fed induction generator," *Renewable Pawer Generation, IET*, vol. 7, no. 6, pp. 631 – 638, 2013.

[11] S. Abdi, E. Abdi, A. Oraee, and R. McMahon, "Equivalent circuit parameters for large brushless doubly fed machines," *IEEE Transactions on Energy Conversion*, vol. 29, no. 6, pp. 706 – 715, 2014.

[12] D. Mathekga, "Field distribution characteristics, non-linear characteristics, and thermal model of the brushless doubly fed (induction) machine," Ph.D. dissertation, University of Cambridge, Engineering Department, 2014.

[13] X. Wang, R. A. McMahon, and P. J. Tavner, "Design of the brushless doubly-fed (induction) machine." Turky: IEEE International Conference on Electric Machines and Drive (IEMDC), May 2007, pp. 1508 – 1513.

[14] R. McMahon, P. Tavner, E. Abdi, P. Malliband, and D. Barker, "Characterising brushless doubly fed machine rotors," *IET Electric Power Applications*, vol. 7, pp. 535 – 543, 2013.

[15] R. A. McMahon, E. Abdi, P. Malliband, S. Shao, M. E. Mathekga, and P. J. Tavner, "Design and testing of a 250 kw brushless dfig." Bristol, UK: 6th IET International Conference on Power Electronics, Machines and Drives (PEMD), March 2012.

[16] F. Creedy, "Some developments in multi-speed cascade induction motors," *Institute of Electrical Engineers Journal*, pp. 511–537, 1920.

[17] Y. Liao, L. Xu, and L. Zheng, "Design of a doubly fed reluctance motor for adjustable speed drives," *IEEE Transactions on Industry Applications*, vol. 32, no. 5, pp. 1195 – 1203, September 1996.

[18] S. Williamson and A. C. Ferreira, "Generalised theory of the brushless doubly-fed machine. part 2: Model verification and performance," *Electrical Power Applications, IEE Proceedings*, vol. 144, pp. 123–129, 1997.

[19] S. Williamson, A. C. Ferreira, and A. K. Wallace, "Generalised theory of the brushless doubly-fed machine. part 1: Analysis," *Electrical Power Applications, IEE Proceedings*, vol. 144, pp. 111–122, 1997.

[20] A. M. Oliveira, P. Kuo-Peng, N. Sadowski, F. Runcos, R. Carlson, and P. Dular, "Finite-element analysis of a double-winding induction motor with a special rotor bars topology," *IEEE Transactions on Magnetics*, vol. 40, no. 2, pp. 770–773, March 2004.

[21] E. Abdi, "Modelling and instrumentation of brushless doubly-fed (induction) machines," Ph.D. dissertation, University of Cambridge, Engineering Department, 2006.

[22] M. G. Say, *The Performance and Design of Alternating Current Machines*, 2nd ed. Sir Isaac Pitman & Sons Ltd., 1948.

[23] J. Pyrhonen, T. Jokinen, and V. Hrabovcova, *Design of rotating electrical machines*. Finland: John Wiley & Sons Inc., 2007.

[24] F. Xiong and X. Wang, "Design of a low-harmonic-content wound rotor for the brushless doubly fed generator," *IEEE Trans. Energy Conversion*, vol. 29, no. 1, pp. 158 – 168, 2014.

Salman Abdi received his BSc degree from Ferdowsi University, Mashhad, Iran, in 2009 and M.S.c degree from Sharif University of Technology in 2011, both in electrical engineering. He is currently working toward the PhD degree at Cambridge University in electrical machines design and modelling. His main research interests include electrical machines and drives for renewable power generation

Ehsan Abdi (SM' 2012) received his BSc degree from Sharif University of Technology in 2002 and his MPhil and PhD degrees from Cambridge University in 2003 and 2006 respectively, all in Electrical Engineering. Currently, he is the Managing Director of Wind Technologies Ltd where he has been involved with commercial exploitation of the brushless doubly fed induction generator technology for wind power applications. His main research interests include electrical machines and drives, renewable power generation, and electrical measurements and instrumentation.

Ashknaz Oraee received her B.Eng. degree in electrical engineering from Kings College London 2011. She is currently working toward the PhD degree at Cambridge University in electrical machine design and optimisation. Her research interests include electrical machines and drives for renewable power generation.

Richard McMahon received the degrees of BA (in Electrical Sciences) and PhD from Cambridge University in electrical engineering, in 1976 and 1980 respectively. Following postdoctoral work on semiconductor device processing he was appointed University Lecturer in Electrical Engineering at Cambridge University Engineering department in 1989 and became a Senior Lecturer in 2000. His research interests include electrical drives, power electronics and semiconductor materials.